

Current constraints on early and stressed dark energy models and future 21 cm perspectives

Maria Archidiacono,¹ Laura Lopez-Honorez,² and Olga Mena³

¹*Department of Physics and Astronomy, Aarhus University, 8000 Aarhus C, Denmark.*

²*Theoretische Natuurkunde,*

*Vrije Universiteit Brussel and The International Solvay Institutes,
Pleinlaan 2, B-1050 Brussels, Belgium.*

³*Instituto de Física Corpuscular (IFIC), CSIC-Universitat de Valencia, E-46071, Spain.*

Despite the great progress of current cosmological measurements, the nature of the dominant component of the universe, coined *dark energy*, is still an open question. *Early Dark Energy* is a possible candidate which may also alleviate some fine tuning issues of the standard paradigm. Using the latest available cosmological data, we find that the 95% CL upper bound on the early dark energy density parameter is $\Omega_{\text{eDE}} < 0.009$. On the other hand, the dark energy component may be a stressed and inhomogeneous fluid. If this is the case, the effective sound speed and the viscosity parameters are unconstrained by current data. Future omniscience-like 21 cm surveys, combined with present CMB data, could be able to distinguish between standard quintessence scenarios from other possible models with 2σ significance, assuming a non-negligible early dark energy contribution. The precision achieved on the Ω_{eDE} parameter from these 21 cm probes could be below $\mathcal{O}(10\%)$.

PACS numbers: 95.36.+x

I. INTRODUCTION

The nature of the mysterious dark energy component that currently dominates the energy content of the universe reveals new physics missing from our universe's picture, and constitutes the fundamental key to understand the fate of the universe. The most economical explanation of the dark energy component attributes this energy density to the one of the vacuum, i.e., a cosmological constant scenario. Together with cold dark matter (CDM), the so-called Λ CDM scenario can account for present data with a flat universe made up of roughly 30% dark matter and 70% dark energy. In this minimal model, the dark energy equation of state, w , which corresponds to the ratio of the dark energy pressure to the dark energy density, is constant and equal to -1 . However, this simple picture suffers from severe fine tuning theoretical issues (see Ref. [1] and references therein) as well as from problems with observations related to the matter power spectrum on scales of a few Mpc and below [2–7]. Possible alternatives to alleviate them have been extensively explored. Perfect dark energy fluids, characterised either by a constant ($w \neq -1$) or by a time varying dark energy equation of state $w(a(t))$, or scalar field models, are the most popular options considered in the cosmological data analyses, as their parameterizations require few extra parameters (two at most) to be added to the usual Λ CDM scenario.

There exists also alternative scenarios, in which the gravitational sector is modified, leading to a modification of Einstein's equations of gravity on large scales. Modifications of gravity (see e.g. [8] and references therein) incorporate models with extra spatial dimensions or an action which is non-linear in the Ricci scalar. There are also non-perfect fluid models, as Chaplygin gas cosmologies [9], which involve more parameters than just one

equation of state w . Of particular interest here is the *Early Dark Energy* (hereafter EDE) case, as it arises as a natural hypothesis of dark energy [10–13]. EDE differs from the cosmological constant because it is not negligible in the early universe and the contribution depends on the initial density parameter Ω_{eDE} . Furthermore, the EDE model considered here is based on a generic dark energy fluid which is inhomogeneous. Density and pressure are time varying, therefore the equation of state is not constant in time. The phenomenological analyses of these inhomogeneous dark energy models usually require additional dark energy clustering parameters, i.e. the dark energy effective sound speed and the dark energy anisotropic stress. The sound speed c_{eff}^2 [14–16] is defined as the ratio between the dark energy pressure perturbation and the dark energy density contrast in the rest frame of the fluid, $c_{\text{eff}}^2 \equiv (\delta P / \delta \rho)_{\text{rest}}$. In the simplest quintessence models, $c_{\text{eff}}^2 = 1$, while the anisotropic stress is zero. The effective sound speed determines the clustering properties of dark energy and consequently it affects the growth of matter density fluctuations. Therefore, in principle, its presence could be revealed in large scale structure observations. The growth of perturbations can also be affected by the anisotropic stress contributions [14, 15, 17] which lead to a damping in the velocity perturbations. In the parametrization used here, the damping effect is driven by the viscosity parameter c_{vis}^2 which links the anisotropic stress to the velocity perturbation and the metric shear.

Despite the precision achieved by the combination of Cosmic Microwave Background (CMB) measurements from the Planck satellite [18], Baryon Acoustic Oscillation (BAO) data from a number of galaxy surveys [19–23] and Supernovae Ia luminosity distance measurements [24] in the extraction of the dark energy equation of state parameter, $w = -1.06 \pm 0.06$ at 68% CL [19], the

nature of the dark energy component remains unknown. Therefore, it is mandatory to carefully study other possibilities including the one of an EDE component, as well as the clustering properties of the dark energy fluid. In this paper we shall address both issues, relaxing the perfect fluid assumption and considering current cosmological data, in addition to the recent BICEP2 measurements of the B-modes power spectrum [25].

We also explore the possibility of constraining an EDE component and/or a stressed dark energy fluid with future 21 cm surveys. The next generation of radio experiments, which will image the neutral intergalactic medium (IGM) in 21 cm emission/absorption, will provide a unique probe of the universe at higher redshifts ($z > 6$) which lie out of the reach of galaxy surveys and CMB experiments. The 21 cm line signal presents several advantages compared to traditional cosmic and astrophysical probes, see e.g. [26], and it could be used to test the nature of dark energy [27]. The future generation of radio interferometers testing the 21 cm signal, including the Squared Kilometer Array (SKA) [28] and omniscopes [29, 30], may provide extra constraints on the cosmological parameters probing the Epoch of Reionisation (EoR) or the high redshift window, see e.g. [31, 32]. In addition, the 21 cm signal can also be used at low redshifts ($z < 5$), offering a competitive cosmological probe for unraveling the nature of the component responsible for the present universe's accelerated expansion [33, 34].

The structure of the paper is as follows. Sections II and III describe the early and stressed dark energy models evolution in terms of the background and perturbation variables. In Sec. IV we present the method and data followed in the numerical analyses presented in Sec. V. Section VI addresses the future perspective and constraints from 21 cm surveys by means of a Fisher matrix forecast analysis. Finally, we draw our conclusions in Sec. VII.

II. EARLY DARK ENERGY MODELS

The concept of EDE cosmology was introduced in [10] and studied in several subsequent works following different possible effective parametrizations of the evolution of the dark energy fluid, see e.g. [11, 13, 18, 35]. Here we follow Ref. [11] to describe the evolution of the background dark energy density from the high redshift, constant value Ω_{eDE} until its present-day value Ω_{DE}^0 (assuming a flat universe with $\Omega_{\text{DE}}^0 + \Omega_{\text{m}}^0 = 1$):

$$\Omega_{\text{DE}}(a) = \frac{\Omega_{\text{DE}}^0 - \Omega_{\text{eDE}}(1 - a^{-3w_0})}{\Omega_{\text{DE}}^0 + \Omega_{\text{m}}^0 a^{3w_0}} + \Omega_{\text{eDE}}(1 - a^{-3w_0}). \quad (1)$$

The evolution of $w(a)$ in this EDE parametrization reads

$$w(a) = -\frac{1}{3[1 - \Omega_{\text{DE}}(a)]} \frac{d \ln \Omega_{\text{DE}}(a)}{d \ln a} + \frac{a_{\text{eq}}}{3(a + a_{\text{eq}})}, \quad (2)$$

where a_{eq} is the scale factor at matter-radiation equality era. The time dependent equation of state $w(a)$ typically

traces the dominant component of the universe at each epoch: first $w \simeq 1/3$ during the radiation dominated period, then $w \simeq 0$ during the matter dominated era and finally $w \rightarrow w_0$ in the present epoch. The current value of the equation of state parameter w_0 might be different* from -1 .

III. STRESSED DARK ENERGY MODELS

Using the notation of Ref. [37] and assuming the synchronous gauge, we follow [13] to describe the dark energy scalar perturbation evolution equations in Fourier space for the density contrast (δ), the velocity divergence (θ) and the anisotropic stress perturbation (σ):

$$\frac{\dot{\delta}}{1+w} = -\left[k^2 + 9\left(\frac{\dot{a}}{a}\right)^2 \left(c_{\text{eff}}^2 - w + \frac{\dot{w}}{3(1+w)(\dot{a}/a)} \right) \right] \frac{\theta}{k^2} - \frac{\dot{h}}{2} - 3\frac{\dot{a}}{a}(c_{\text{eff}}^2 - w)\frac{\delta}{1+w}; \quad (3)$$

$$\dot{\theta} = -\frac{\dot{a}}{a}(1 - 3c_{\text{eff}}^2)\theta + \frac{\delta}{1+w}c_{\text{eff}}^2k^2 - k^2\sigma; \quad (4)$$

$$\dot{\sigma} = -3\frac{\dot{a}}{a}\left[1 - \frac{\dot{w}}{3w(1+w)(\dot{a}/a)} \right] \sigma + \frac{8c_{\text{vis}}^2}{3(1+w)} \left[\theta + \frac{\dot{h}}{2} + 3\dot{\eta} \right], \quad (5)$$

where c_{eff}^2 denotes the effective sound speed. In the last equation, the velocity and the metric shear (sometimes referred to as $H_T = -(h/2 + 3\eta)$) are related to the dark energy shear stress through the viscosity parameter c_{vis}^2 . The latter relation was first introduced in Ref. [15][†] and relates directly the anisotropic stress with the damping of velocity fluctuations on shear-free frames ($H_T = 0$), if $c_{\text{vis}}^2 > 0$. We have also addressed the contribution of the dark energy shear stress to the evolution equations for the tensor perturbations.

The differential equations above govern the clustering properties of the dark energy fluid, and we shall solve them and compare the results to current and future observations using the methods detailed in the following sections.

IV. METHOD AND DATA FOR CURRENT CONSTRAINTS

We have modified the latest version of the Boltzmann equations solver CAMB [38] in order to account for

* Notice that the clustering properties of a universe with $-1 < w < -1/3$ deviate from those of a Λ CDM universe with $w = -1$ and therefore it can be inconsistent with observations [36].

[†] Note that σ here is related to the variable π in [14] through the relation $\sigma = (2/3)\pi/(1+w)$.

Eqs. (1)-(5).

The parameter space contains the six standard parameters of the Λ CDM model

$$\{\Omega_b h^2, \Omega_c h^2, \theta, \tau, n_s, \ln(10^{10} A_s)\}, \quad (6)$$

where $\Omega_b h^2 = \omega_b$ is the present physical energy density in baryons, $\Omega_c h^2 = \omega_c$ is the present physical cold dark matter energy density, θ is the angular scale of the sound horizon, τ is optical depth to reionisation and n_s and A_s are the spectral index and the amplitude of primordial scalar perturbations at a pivot scale $k = 0.05 \text{ Mpc}^{-1}$, respectively.

Since we include tensor perturbations, we have also considered the tensor-to-scalar ratio r parameter, defined relatively to the same pivot scale of the scalar perturbations, $k = 0.05 \text{ Mpc}^{-1}$. Finally, we include all the parameters describing the EDE model evolution (see Secs. II and III):

$$\{\Omega_{\text{eDE}}, w_0, c_{\text{vis}}^2, c_{\text{eff}}^2\}. \quad (7)$$

We assume flat priors on the parameters as listed in Tab. I. The sampling of the parameter space is performed through the Monte Carlo Markov Chain (MCMC) public package CosmoMC [39].

Parameter	Prior
$\Omega_b h^2$	0.005 \rightarrow 0.1
$\Omega_c h^2$	0.01 \rightarrow 0.99
θ	0.5 \rightarrow 10
τ	0.01 \rightarrow 0.8
n_s	0.5 \rightarrow 1.5
$\ln(10^{10} A_s)$	2.7 \rightarrow 4
r	0 \rightarrow 1
Ω_{eDE}	0 \rightarrow 0.1
w_0	-1 \rightarrow 0
c_{eff}^2	0 \rightarrow 1
c_{vis}^2	0 \rightarrow 1

TABLE I: Range of the flat priors for the cosmological parameters considered here.

The Bayesian inference is based on the CMB temperature anisotropy power spectrum of the Planck experiment, implemented following the prescriptions of Ref. [40]. We have also considered the CMB polarization measurements from the nine-year data release of the WMAP satellite [41]. In the following, we shall refer to the former data as WP. The maximum multipole number of the Planck temperature power spectra is $\ell_{\text{max}} = 2500$. The WP measurements reach a maximum multipole $\ell = 23$, see Ref. [41]. In order to directly constrain the tensor-to-scalar ratio r , the nine-bins measurements of the B-modes polarization power spectrum from the BICEP-2 collaboration[25] are included.

V. CURRENT COSMOLOGICAL CONSTRAINTS

In this section we apply the data sets described above, using the MCMC method, to four possible scenarios:

- **Case 1:** In this scenario, both the early dark energy component Ω_{eDE} and the dark energy perturbation parameters c_{eff}^2 and c_{vis}^2 are free parameters, with the priors specified in Tab. I. We also consider in this case the current value of the dark energy equation of state, w_0 , see Eq. (1), as a free parameter.
- **Case 2:** The early dark energy component Ω_{eDE} and w_0 are free parameters, but the dark energy perturbations are fixed to their standard values: $c_{\text{eff}}^2 = 1$ and $c_{\text{vis}}^2 = 0$ (i.e. no anisotropic stress contribution is considered in this case).
- **Case 3:** We consider no early dark energy component ($\Omega_{\text{eDE}} = 0$) but the dark energy perturbations c_{eff}^2 and c_{vis}^2 are both free parameters, varying with a flat prior in the range $[0, 1]$, as well as a constant dark energy equation of state w , which varies with a prior in the range $[-1, 0]$.
- **Case 4:** We consider a simple w CDM cosmology, i.e., a cosmological scenario with a constant dark energy equation of state, which is allowed to freely vary in the range $[-1, 0]$.

Table II shows the mean values with 1σ errors and the 2σ upper bounds for the EDE parameters following the case order listed above. Notice first that we do not show the values for the dark energy perturbation parameters (c_{eff}^2 and c_{vis}^2), since current CMB measurements are unable to constrain them. Secondly, when setting $c_{\text{eff}}^2 = 1$ and $c_{\text{vis}}^2 = 0$ (see Case 2 above), we find an upper limit on the early dark energy parameter $\Omega_{\text{eDE}} < 0.012$ at 95% CL. The former bound is looser than the one reported by the Planck collaboration, $\Omega_{\text{eDE}} < 0.010$ at 95% CL with the same data sets (Planck temperature and WP data). The larger value that we get on Ω_{eDE} is related to the degeneracy between this parameter and the tensor-to-scalar ratio r , as we shall explain below. The addition of the BICEP2 data makes our 95% CL upper limit on Ω_{eDE} tighter ($\Omega_{\text{eDE}} < 0.009$ at 95% CL). When allowing the dark energy perturbations c_{eff}^2 and c_{vis}^2 to be free parameters (Case 1 above), the 95% CL upper bound Ω_{eDE} degrades but not significantly: we find $\Omega_{\text{eDE}} < 0.015$ ($\Omega_{\text{eDE}} < 0.010$) at 95% CL before (after) combining Planck and WP measurements with BICEP2 data.

In general, the results for the standard Λ CDM cosmological parameters do not deviate significantly from their expected mean values and errors. This can be noticed by comparing the first three cases depicted in Tab. II with the last rows, which show the expectations within the w CDM cosmological scenario. Indeed, the current value

	Planck+ WP	Planck +WP + BICEP-2
Case 1		
Ω_{eDE}	< 0.015	< 0.010
w_0	< -0.658	< -0.722
r	< 0.09	0.15 ± 0.04
n_s	0.960 ± 0.008	0.963 ± 0.007
Case 2		
$\Omega_{\text{eDE}}(c_{\text{eff}}^2 = 1, c_{\text{vis}}^2 = 0)$	< 0.012	< 0.009
$w_0(c_{\text{eff}}^2 = 1, c_{\text{vis}}^2 = 0)$	< -0.659	< -0.722
r	< 0.10	0.16 ± 0.04
n_s	0.960 ± 0.007	0.963 ± 0.008
Case 3		
Ω_{eDE}	0	0
w	< -0.647	< -0.709
r	< 0.11	0.16 ± 0.04
n_s	0.960 ± 0.007	0.964 ± 0.007
Case 4		
$\Omega_{\text{eDE}}(c_{\text{eff}}^2 = 1, c_{\text{vis}}^2 = 0)$	0	0
$w(c_{\text{eff}}^2 = 1, c_{\text{vis}}^2 = 0)$	< -0.655	< -0.705
r	< 0.11	0.16 ± 0.04
n_s	0.960 ± 0.008	0.964 ± 0.007

TABLE II: Mean values with 1σ errors and 2σ upper bounds for the Ω_{eDE} parameter as well as for the most correlated cosmological parameters for the different possible cases described in Sec. V. The dark energy perturbation parameters c_{eff}^2 and c_{vis}^2 are not listed in this table, as current cosmological data are unable to constrain them.

of the dark energy equation of state w_0 does not show a very strong dependence on the dark energy perturbation parameters, as its 95% CL upper bound remains unaffected when c_{eff}^2 and c_{vis}^2 are both freely varying. Concerning the value of n_s , its mean value is strongly affected when including BICEP2 data in our numerical analyses, regardless of the dark energy scenario.

Figure ?? shows the marginalised 2D plots and the posteriors involving the most relevant cosmological parameters here in the case in which both the early dark energy component Ω_{eDE} and the perturbation parameters c_{eff}^2 and c_{vis}^2 are allowed to vary freely (see Case 1 above). The red contours refer to the results arising from the analysis of Planck + WP data, while the blue contours include BICEP2 as well. The marginalised 2D plot in the bottom left corner, in the (Ω_{eDE}, r) plane, shows the degeneracy between the EDE component and the tensor-to-scalar ratio r . There exists a mild anti-correlation between these two parameters, which can be easily understood: both parameters show an effect at very large scales, increasing the power at very low multipoles. As the BICEP2 data constrain r to be different from zero, the 2σ upper bound on Ω_{eDE} is tighter, in order to compensate the contribution from the tensor modes at large scales. A similar effect can also be noticed in the 2D marginalised plot in the (w_0, r) plane: given the anti-correlation between w_0 and r , the BICEP2 measurements of r reduce the upper bound on w_0 . There also exists a degeneracy between the Ω_{eDE} and w_0 parameters, as can be noticed from the right lower panel of Fig. 1: larger (smaller) values of the present dark energy equation of state, w_0 , allow for smaller (larger) values of the EDE parameter, Ω_{eDE} .

Therefore, these two parameters are anti-correlated, as can be learnt from Eq. (1): for a given value of the Ω_{eDE} parameter and the scale factor a , the quantity Ω_{DE} grows as the value of w_0 does.

VI. 21 CM FORECASTS

In this section, we follow the description of Ref. [32] for the 21 cm brightness background temperature $T_b(z)$, for the evolution equations of the linear perturbation $\delta T_b(z)$ as well as for the reionisation model implementation.

The study of the 21 cm signal requires to deal with the angular location on the sky plane θ , and with the frequency difference Δf of the signal to a central 21 cm line of redshift z . The dual coordinates of this system are denoted by \mathbf{u}_\perp and u_\parallel , and they are related to the standard comoving wavevector \mathbf{k} components as follows:

$$\mathbf{u}_\perp = D_A(z)\mathbf{k}_\perp, \quad u_\parallel = y(z)k_\parallel, \quad (8)$$

where $D_A(z)$ is the angular comoving distance and

$$y(z) = \frac{\lambda_{21}(1+z)^2}{H(z)}, \quad (9)$$

where λ_{21} is the 21 cm wavelength (in the rest frame) and $H(z)$ is the Hubble rate. The 21 cm brightness temperature power spectrum relevant for our analyses, $P_{\delta T_b}(\mathbf{u})$, is related to $P_{\delta T_b}(\mathbf{k})$ as follows:

$$P_{\delta T_b}(\mathbf{u}) = \frac{P_{\delta T_b}(\mathbf{k})}{D_A(z)^2 y(z)}. \quad (10)$$

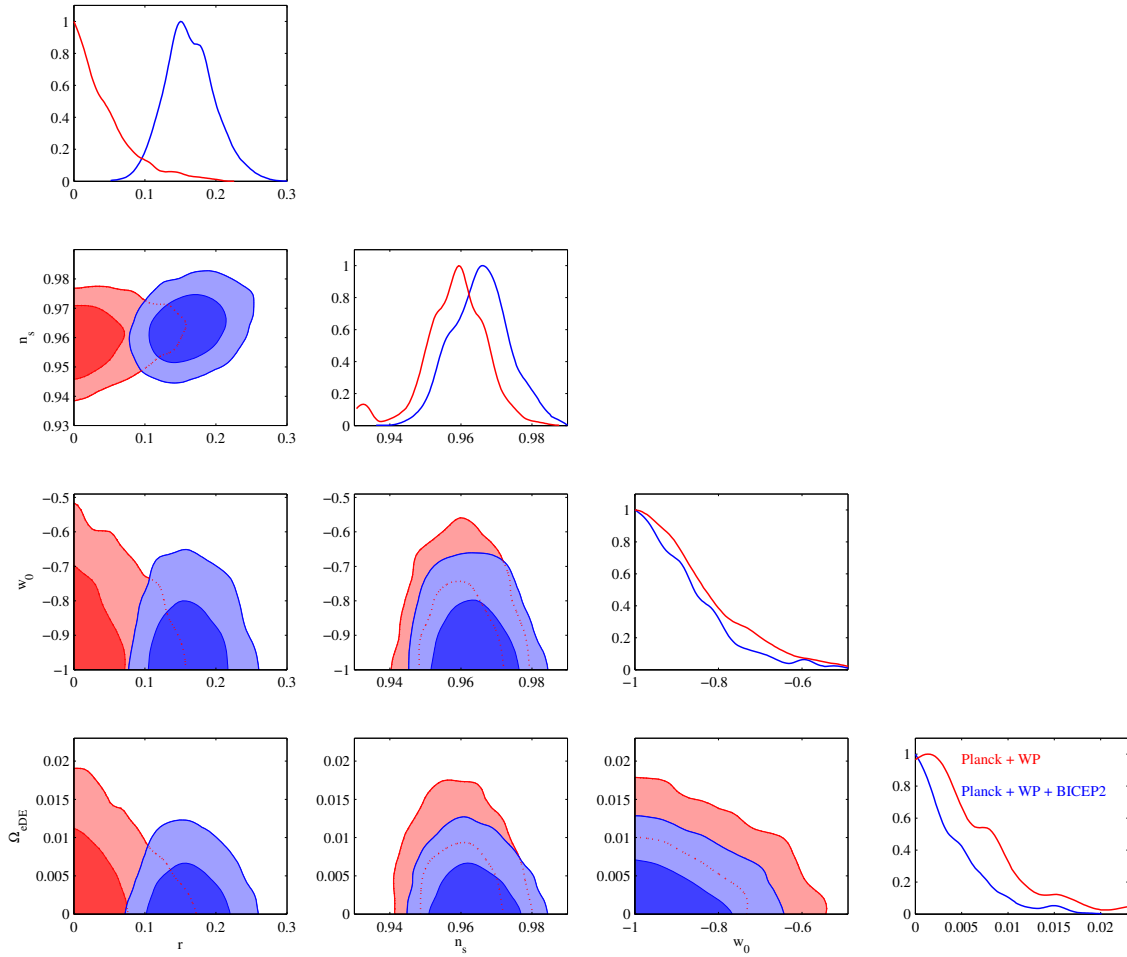


FIG. 1: *2D plots*: Red (Blue) contours show the 68% and 95% CL allowed regions from Planck + WP (Planck + WP + BICEP2). *1D plots*: Red (Blue) lines depict the marginalised one-dimensional posteriors from Planck + WP (Planck + WP + BICEP2) measurements. In this case, both the dark energy perturbation parameters and the EDE component are free parameters (see Case 1 of Tab. II). BICEP2 measurements point towards a non-zero value of r . As a consequence, since Ω_{eDE} and r are anti-correlated, the constraints on Ω_{eDE} are tighter when considering BICEP2 data in the numerical analyses (see the results depicted in Tab. II).

For the Fisher matrix analysis, we have adopted the formalism of Refs. [31, 32]. Assuming that $P_{\delta T_b}(\mathbf{u})$ is gaussian-distributed, we can approximate the Fisher matrix by

$$F_{ab} = \frac{1}{2} \sum_{\mathbf{u}_{\parallel}, \mathbf{u}_{\perp}} \frac{N_c}{[P_{\delta T_b}(\mathbf{u}) + P_{\text{noise}}]^2} \frac{\partial P_{\delta T_b}(\mathbf{u})}{\partial \lambda_a} \frac{\partial P_{\delta T_b}(\mathbf{u})}{\partial \lambda_b}, \quad (11)$$

where $\lambda_{a,b}$ are the cosmological parameters involved in the Fisher forecast analysis, and

$$N_c = \frac{4\pi f_{\text{sky}}}{\Theta^2} 2\pi k_{\perp} \delta k_{\perp} \delta k_{\parallel} \frac{V}{(2\pi)^3}, \quad (12)$$

is the number of independent cells probed for a given value of \mathbf{u} (or \mathbf{k}), V is the comoving volume covered and Θ is the angular patch in the sky[‡]. In Eq. (11), P_{noise} is given by [32, 42]:

$$P_{\text{noise}}(\mathbf{u}) \simeq \frac{4\pi f_{\text{sky}}}{\Omega_{\text{fov}}} \frac{\lambda^2}{D^2 f_{\text{cover}}^2} \frac{T_{\text{sys}}^2}{B W t_{\text{obs}}}, \quad (13)$$

with f_{sky} the fraction of the sky covered by the survey,

[‡] Θ is taken to be lower than 1 rad to be in agreement with the flat-sky approximation.

Ω_{fov} the field of view, λ the redshifted wavelength of the signal, T_{sys} the system temperature, D the size of the array, B_W the experiment's bandwidth and f_{cover} the covering factor of the array. Beam effects at small scales can be incorporated by multiplying Eq. (13) by the factor $\exp[\mathbf{u}_{\perp}^2/(4\sqrt{\ln 2}/\theta_{fw})^2]$, with $\theta_{fw} = 0.89\lambda/D$, see Ref. [32].

In what follows, we consider two possible 21 cm experiment configurations. The first one is a CHIME-like [43] experiment, covering a low redshift range $0.8 < z < 2.5$. In our analyses we use a setup similar to the one considered in [34]. The second one is an omniscopes-like instrument sensitive to the EoR. In the latter case, we follow the setup of Ref. [32]. In our treatment of the Fisher matrix, we use a convolution of the signal with the frequency window function associated with the mean redshift of observation. This method helps in reducing the degeneracy between the cosmological parameters τ and $\ln(A_S)$ when considering one single redshift slice for an omniscopes-like experiment [32]. Notice that, in what follows, we shall assume that most of the foregrounds can be eliminated, assumption which is still under active research (see e.g. [44]). We also neglect the fact that ionising sources could affect the 21cm perturbations, providing extra contributions to the power spectrum [31, 32]. Therefore the analysis presented here should be regarded as an optimistic appraisal of the 21 cm signal potential to constrain both an EDE component and its clustering properties.

We present results for two fiducial cosmological models: the fiducial model 1 (2) with $\Omega_{\text{eDE}} = 0.01$ (0.03), $c_{\text{vis}}^2 = 0$ (0.33) and $c_{\text{eff}}^2 = 1$ (0.33), both of them assuming the same value for the dark energy equation of state at present, $w_0 = -0.9$. Figure 2 shows the evolution of the background quantities $\Omega_{\text{DE}}(z)$ and $w(z)$, see Eqs. (1) and (2), as a function of the redshift, for these two possible fiducial cosmologies. The redshift ranges tested by the two possible 21 cm future experiments considered here are depicted by the grey rectangular zones. Notice that both experiments are located where the difference among the expansion histories for these two fiducial models is non-negligible. Therefore, one would expect to have sensitivity to distinguish between different cosmological backgrounds when exploring the 21 cm power spectrum in the two redshift ranges depicted in Fig. 2.

A. CHIME $0.8 < z < 2.5$

In Tab. III, we provide the value of the parameters specifying the CHIME experiment considered in our analyses, which are similar to those considered in Ref. [34]. For the system temperature, we have taken $T_{\text{sys}} = [40 + 5(\nu/710\text{Mhz})^{-2.6}]$ K, where ν is the redshifted frequency of the 21 cm signal. We have also considered a comoving number density of sources of $0.03h^3\text{Mpc}^{-3}$, contributing to shot-noise.

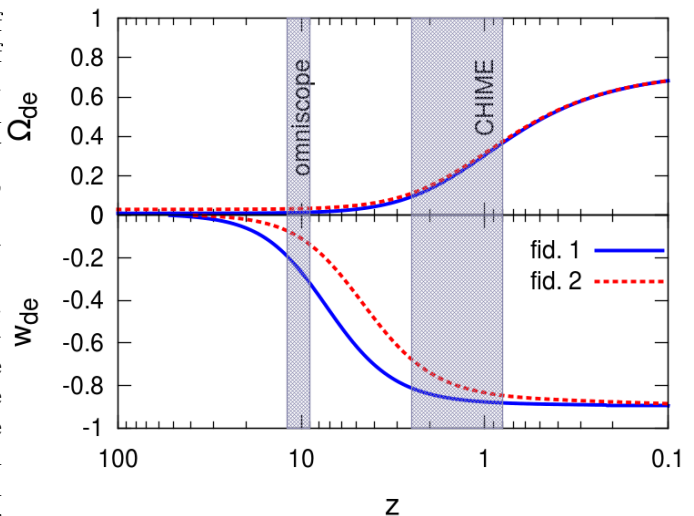


FIG. 2: Evolution of the background quantities for the fiducial models of Tabs. IV and VI. The redshift ranges tested by the 21 cm experiments considered here are shown by the grey rectangular areas.

redshift slices	B_W	D	f_{cover}	t_{obs}	f_{sky}
0.8/1/2/2.5	2 Mhz	100 m	1	1 yr	0.5

TABLE III: Specifications of the CHIME-like experiment, see also Ref. [34].

The results for the two possible fiducial models described in the previous section are presented in Tab. IV, using $u_{\perp}^{\text{min}} = 2\pi/\theta_{res}(z)$ with $\theta_{res} = \lambda_{21}(1+z)/D$. Notice that the CHIME configuration can provide a high precision measurement of w_0 . However, the precision in the extraction of the EDE background parameter Ω_{eDE} , as well as in the measurements of the dark energy clustering parameters c_{vis}^2 and c_{eff}^2 , is quite poor. Concerning the standard cosmological parameters, the constraints on both $\ln A_s$ and $\Omega_b h^2$ are worse than those obtained with current CMB data. Indeed, these two parameters affect the overall amplitude of the 21 cm signal, while the CMB amplitude signal is mainly driven by the $\ln A_s$ parameter, with $\Omega_b h^2$ controlling the CMB even-odd peak ratio. However, the constraints on both τ and n_s are tighter for the 21 cm experiment. Let us emphasise that the addition of BICEP2 data does not change the results presented here.

B. Omniscopes $z > 7$

We provide in Tab. V the specifications of the future omniscopes-like experiment explored here. Table VI shows the 1σ errors for the two fiducial models previously

	fiducial ₁ (fiducial ₂)	CHIME	CHIME + Planck & WP
$\Omega_b h^2$	0.02258	$2.07 (2.15) \cdot 10^{-3}$	$2.55 (2.22) \cdot 10^{-4}$
h	0.71	$1.4 (2.21) \cdot 10^{-2}$	$0.88 (1.11) \cdot 10^{-2}$
$\Omega_c h^2$	0.1109	$7.07 (9.57) \cdot 10^{-3}$	$1.54 (1.66) \cdot 10^{-3}$
Ω_{eDE}	0.01 (0.03)	$1.92 (2.97) \cdot 10^{-2}$	$3.31 (3.8) \cdot 10^{-3}$
c_{vis}^2	0. (0.33)	13.6 (2.24)	$2.82 (2.63) \cdot 10^{-1}$
w_0	-0.9	$5.35 (7.78) \cdot 10^{-2}$	$2.65 (3.23) \cdot 10^{-2}$
c_{eff}^2	1. (0.33)	0.214 (1.41)	$2.89 (2.72) \cdot 10^{-1}$
n_s	0.963	$1.9 (3.63) \cdot 10^{-2}$	$5.26 (5.32) \cdot 10^{-3}$
τ	0.088	$2.78 (2.69) \cdot 10^{-3}$	$7.14 (6.79) \cdot 10^{-4}$
$\ln[10^{10} A_s]$	3.09784	$7.32 (8.26) \cdot 10^{-1}$	$2.44 (2.44) \cdot 10^{-2}$

TABLE IV: 1σ errors on the parameters describing the two fiducial models here, which only differ in the values of the Ω_{eDE} and the dark energy clustering parameters.

redshift slices	B_W	D	f_{cover}	t_{obs}	f_{sky}
9/10/11/12	10 Mhz	10 km	0.1	1 yr	0.5

TABLE V: Specifications of the omniscopy-like experiment for which we have considered 10^6 antennas, see also Ref. [32].

illustrated for the CHIME-like experiment [§]. While the $\Omega_b h^2$ parameter can be measured with a precision similar to the one achieved with current CMB data, the $\ln A_s$ parameter is still better constrained by the latter measurements. For the setup and the fiducial model considered here, the errors on τ and n_s are significantly better than for CMB experiments, see also the discussion in Ref. [32]. The addition of Planck and/or the BICEP2 priors does not change much the overall picture for the marginalised errors depicted in Tab. V. Let us emphasise that we did not take into account extra ionising sources that can severely damage the variances of the reionisation model parameters, see e.g. [31, 32].

Concerning the dark energy parameters, the constraints on the background parameters w_0 and Ω_{eDE} reach high precision levels, with 2% and 7% (6%) errors, respectively, for $\Omega_{eDE} = 0.01(0.03)$. A similar precision on the measurement of the dark energy clustering parameters c_{eff}^2 and c_{vis}^2 is obtained with future 21 cm measurements, except for the case in which $c_{vis}^2 = 0$ and $c_{eff}^2 = 1.0$. For this particular scenario, the constraint on c_{eff}^2 is very poor.

Figure 3 shows the two-dimensional 1 and 2σ allowed regions in a reduced number of parameters for the fiducial scenario with $\Omega_{eDE} = 0.01$, $c_{vis}^2 = 0$ and $c_{eff}^2 = 1.0$. The top panel of Fig. 3 illustrates the expected correlation in the (w_0, n_s) plane. As in the case of the analysis of Sec. V, Ω_{eDE} and w_0 are anti-correlated, and therefore there exists a mild anti-correlation between Ω_{eDE} and n_s ,

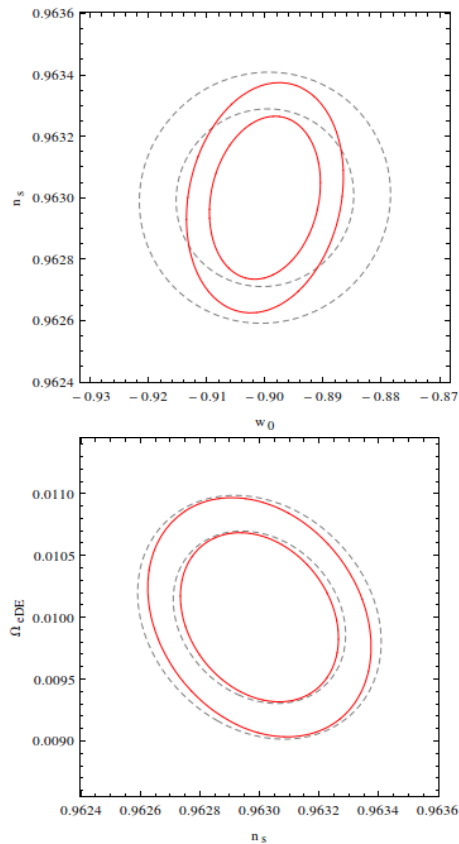


FIG. 3: 1 and 2σ allowed regions from the Fisher analysis with an omniscopy-like experiment with four redshift slices $z = 9, 10, 11, 12$ for the fiducial model 1. The addition of the Planck measurements results in the continuous red contours.

[§] In this case, we have also marginalised over the parameter Δ_z specifying the duration of the reionisation process, see [32] for more details on the background reionisation model.

as depicted in the bottom panel of Fig. 3. We also depict in red solid lines the resulting contours after adding the Planck measurements.

	fiducial ₁ (fiducial ₂)	Omniscope	Omniscope + Planck & WP
$\Omega_b h^2$	0.02258	$2.85 (5.75) \cdot 10^{-5}$	$2.64 (4.79) \cdot 10^{-5}$
h	0.71	$5.51 (5.54) \cdot 10^{-3}$	$3.39 (3.78) \cdot 10^{-3}$
$\Omega_c h^2$	0.1109	$2.51 (5.73) \cdot 10^{-4}$	$2.44 (4.65) \cdot 10^{-4}$
Ω_{eDE}	0.01 (0.03)	$0.697 (1.6) \cdot 10^{-3}$	$0.684 (1.47) \cdot 10^{-3}$
c_{vis}^2	0. (0.33)	$1.93 (1.4) \cdot 10^{-1}$	$1.59 (1.21) \cdot 10^{-1}$
w_0	-0.9	$1.53 (1.56) \cdot 10^{-2}$	$0.953 (1.09) \cdot 10^{-2}$
c_{eff}^2	1. (0.33)	1.78 (0.22)	$2.86 (1.7) \cdot 10^{-1}$
n_s	0.963	$2.89 (4.27) \cdot 10^{-4}$	$2.65 (3.96) \cdot 10^{-4}$
τ	0.088	$3.11 (3.09) \cdot 10^{-5}$	$3.1 (3.08) \cdot 10^{-5}$
$\log[10^{10} A_s]$	3.09784	$3.34 (3.18) \cdot 10^{-2}$	$1.98 (1.94) \cdot 10^{-2}$
Δ_z	1.5	$8.39 (8.8) \cdot 10^{-4}$	$8.38 (8.79) \cdot 10^{-4}$

TABLE VI: As Tab. IV but for the omniscope-like experiment considered here, see also Ref. [32].

VII. SUMMARY AND CONCLUSIONS

In the last few years Cosmic Microwave Background (CMB) measurements have reached an extremely high sensitivity, allowing for high precision cosmology and providing, therefore, very tight constraints on the basic parameters governing the standard Λ CDM model. The recent claimed detection of primordial B-modes from the BICEP2 experiment has also offered new insights in cosmology. Here we have exploited the former signal, together with the latest CMB measurements, to update the constraints on an Early Dark Energy component. We find $\Omega_{eDE} < 0.009$ at 95% CL when Planck, WMAP polarization and BICEP2 data are considered, assuming that the early dark energy component can be described by a perfect fluid. If the former assumption is relaxed, and the dark energy perturbation parameters c_{eff}^2 and c_{vis}^2 are allowed to vary freely, Ω_{eDE} turns out to be less well constrained. Furthermore we find that current CMB measurements are unable to constrain c_{eff}^2 and c_{vis}^2 .

In this case, future cosmological measurements of the 21 cm line can be crucial. In the optimistic approach followed here (i.e. in the absence of foregrounds or extra ionising sources), our Fisher matrix analyses of future data from an omniscope-like experiment show that the combination of these 21 cm cosmological probes and current CMB measurements will be able to distinguish be-

tween the canonical quintessence scenario (characterised by $c_{eff}^2 = 1$ and $c_{vis}^2 = 0$) and other possible models (with non standard clustering parameters, as, for instance, with $c_{eff}^2 = 0.33$ and $c_{vis}^2 = 0.33$) with 2σ significance, in the presence of a non-negligible early dark energy component Ω_{eDE} . The errors on the energy density of the former parameter from the joint analysis of future 21 cm data and current CMB measurements, assuming $\Omega_{eDE} = 0.01 (0.03)$, are $0.684 (1.47) \cdot 10^{-3}$. Future 21 cm probes can therefore achieve a precision below 10% in the measurement of an early, non-homogeneous dark energy component.

Acknowledgements

OM is supported by the Consolider Ingenio project CSD2007-00060, by PROMETEO/2009/116, by the Spanish Grant FPA2011-29678 of the MINECO. OM and MA are also partially supported by PITN-GA-2011-289442-INVISIBLES. We also thank the spanish MINECO (Centro de excelencia Severo Ochoa Program) under grant SEV-2012-0249. LLH is supported through an FWO-Vlaanderen post doctoral fellowship project number 1271513. LLH also recognizes partial support from the Strategic Research Program High Energy Physics of the Vrije Universiteit Brussel and from the Belgian Federal Science Policy through the Interuniversity Attraction Pole P7/37 Fundamental Interactions.

-
- [1] E. J. Copeland, M. Sami and S. Tsujikawa, *Int. J. Mod. Phys. D* **15**, 1753 (2006) [hep-th/0603057]; P. J. E. Peebles and B. Ratra, *Rev. Mod. Phys.* **75**, 559 (2003) [astro-ph/0207347]; R. R. Caldwell and M. Kamionkowski, *Annual Review of Nuclear and particle Science* **59**, 397 (2009) [astro-ph/0903.0866].
- [2] B. Moore, T. R. Quinn, F. Governato, J. Stadel and G. Lake, *Mon. Not. Roy. Astron. Soc.* **310**, 1147 (1999) [astro-ph/9903164].
- [3] P. Bode, J. P. Ostriker and N. Turok, *Astrophys. J.* **556**, 93 (2001) [astro-ph/0010389].
- [4] J. Penarrubia, A. Pontzen, M. G. Walker and S. E. Koposov, *Astrophys. J.* **759**, L42 (2012) [arXiv:1207.2772 [astro-ph.GA]].
- [5] M. Boylan-Kolchin, J. S. Bullock and M. Kaplinghat, *Mon. Not. Roy. Astron. Soc.* **422**, 1203 (2012) [arXiv:1111.2048 [astro-ph.CO]].
- [6] I. Ferrero, M. G. Abadi, J. F. Navarro, L. V. Sales and S. Gurovich, *Mon. Not. Roy. Astron. Soc.* **425**, 2817 (2012) [arXiv:1111.6609 [astro-ph.CO]].
- [7] D. H. Weinberg, J. S. Bullock, F. Governato, R. K. de Naray and A. H. G. Peter, arXiv:1306.0913 [astro-ph.CO].
- [8] A. De Felice and S. Tsujikawa, *Living Rev. Rel.* **13**, 3

- (2010) [arXiv:1002.4928 [gr-qc]].
- [9] M. C. Bento, O. Bertolami and A. A. Sen, *Phys. Rev. D* **66**, 043507 (2002) [gr-qc/0202064].
- [10] C. Wetterich, *Phys. Lett. B* **594**, 17 (2004) [astro-ph/0403289].
- [11] M. Doran and G. Robbers, *JCAP* **0606**, 026 (2006) [astro-ph/0601544].
- [12] B. Chang and L. Xu, arXiv:1401.6710 [astro-ph.CO]; V. Pettorino, L. Amendola and C. Wetterich, *Phys. Rev. D* **87**, 083009 (2013) [arXiv:1301.5279 [astro-ph.CO]]; E. Calabrese, D. Huterer, E. V. Linder, A. Melchiorri and L. Pagano, *Phys. Rev. D* **83**, 123504 (2011) [arXiv:1103.4132 [astro-ph.CO]]; L. Hollenstein, D. Sapone, R. Crittenden and B. M. Schaefer, *JCAP* **0904**, 012 (2009) [arXiv:0902.1494 [astro-ph.CO]].
- [13] E. Calabrese, R. de Putter, D. Huterer, E. V. Linder and A. Melchiorri, *Phys. Rev. D* **83**, 023011 (2011) [arXiv:1010.5612 [astro-ph.CO]].
- [14] W. Hu, D. J. Eisenstein, M. Tegmark and M. J. White, *Phys. Rev. D* **59**, 023512 (1999) [astro-ph/9806362].
- [15] W. Hu, *Astrophys. J.* **506**, 485 (1998) [astro-ph/9801234].
- [16] T. Basse, O. E. Bjaelde, S. Hannestad and Y. Y. Y. Wong, arXiv:1205.0548 [astro-ph.CO]; R. de Putter, D. Huterer and E. V. Linder, *Phys. Rev. D* **81**, 103513 (2010) [arXiv:1002.1311 [astro-ph.CO]]; D. Sapone and M. Kunz, *Phys. Rev. D* **80**, 083519 (2009) [arXiv:0909.0007 [astro-ph.CO]].
- [17] L. Amendola, S. Fogli, A. Guarnizo, M. Kunz and A. Vollmer, *Phys. Rev. D* **89**, 063538 (2014) [arXiv:1311.4765 [astro-ph.CO]]; D. Sapone, E. Majerotto, M. Kunz and B. Garilli, *Phys. Rev. D* **88**, 043503 (2013) [arXiv:1305.1942 [astro-ph.CO]]; D. Sapone and E. Majerotto, *Phys. Rev. D* **85**, 123529 (2012) [arXiv:1203.2157 [astro-ph.CO]]; D. F. Mota, J. R. Kristiansen, T. Koivisto and N. E. Groeneboom, *Mon. Not. Roy. Astron. Soc.* **382**, 793 (2007) [arXiv:0708.0830 [astro-ph]]; T. Koivisto and D. F. Mota, *Phys. Rev. D* **73**, 083502 (2006) [astro-ph/0512135].
- [18] P. A. R. Ade *et al.* [Planck Collaboration], arXiv:1303.5076 [astro-ph.CO].
- [19] L. Anderson *et al.* [BOSS Collaboration], arXiv:1312.4877 [astro-ph.CO].
- [20] F. Beutler, C. Blake, M. Colless, D. H. Jones, L. Staveley-Smith, L. Campbell, Q. Parker and W. Saunders *et al.*, *Mon. Not. Roy. Astron. Soc.* **416**, 3017 (2011) [arXiv:1106.3366 [astro-ph.CO]].
- [21] N. G. Busca, T. Delubac, J. Rich, S. Bailey, A. Font-Ribera, D. Kirkby, J. M. Le Goff and M. M. Pieri *et al.*, *Astron. Astrophys.* **552**, A96 (2013) [arXiv:1211.2616 [astro-ph.CO]].
- [22] D. Kirkby, D. Margala, A. Slosar, S. Bailey, N. G. Busca, T. Delubac, J. Rich and M. Blomqvist *et al.*, *JCAP* **1303**, 024 (2013) [arXiv:1301.3456 [astro-ph.CO]].
- [23] A. Slosar, V. Irsic, D. Kirkby, S. Bailey, N. G. Busca, T. Delubac, J. Rich and E. Aubourg *et al.*, *JCAP* **1304**, 026 (2013) [arXiv:1301.3459 [astro-ph.CO]].
- [24] N. Suzuki, D. Rubin, C. Lidman, G. Aldering, R. Amanullah, K. Barbary, L. F. Barrientos and J. Botyanski *et al.*, *Astrophys. J.* **746**, 85 (2012) [arXiv:1105.3470 [astro-ph.CO]].
- [25] P. A. R. Ade *et al.* [BICEP2 Collaboration], arXiv:1403.3985 [astro-ph.CO].
- [26] A. Loeb and M. Zaldarriaga, *Phys. Rev. Lett.* **92**, 211301 (2004) [astro-ph/0312134].
- [27] S. Wyithe, A. Loeb and P. Geil, [arXiv:0709.2955 [astro-ph]]. J. Q. Xia and M. Viel, *JCAP* **0904**, 002 (2009) [arXiv:0901.0605 [astro-ph.CO]].
- [28] G. Mellema, L. V. E. Koopmans, F. A. Abdalla, G. Bernardi, B. Ciardi, S. Daiboo, A. G. de Bruyn and K. K. Datta *et al.*, *Exper. Astron.* **36**, 235 (2013) [arXiv:1210.0197 [astro-ph.CO]].
- [29] M. Tegmark and M. Zaldarriaga, *Phys. Rev. D* **79**, 083530 (2009) [arXiv:0805.4414 [astro-ph]].
- [30] H. Zheng, M. Tegmark, V. Buza, J. S. Dillon, H. Gharibyan, J. Hickish, E. Kunz and A. Liu *et al.*, arXiv:1309.2639 [astro-ph.IM].
- [31] Y. Mao, M. Tegmark, M. McQuinn, M. Zaldarriaga and O. Zahn, *Phys. Rev. D* **78**, 023529 (2008) [arXiv:0802.1710 [astro-ph]].
- [32] S. Clesse, L. Lopez-Honorez, C. Ringeval, H. Tashiro and M. H. G. Tytgat, *Phys. Rev. D* **86**, 123506 (2012) [arXiv:1208.4277 [astro-ph.CO]].
- [33] T. -C. Chang, U. -L. Pen, J. B. Peterson and P. McDonald, *Phys. Rev. Lett.* **100**, 091303 (2008) [arXiv:0709.3672 [astro-ph]].
- [34] A. Hall, C. Bonvin and A. Challinor, *Phys. Rev. D* **87**, no. 6, 064026 (2013) [arXiv:1212.0728 [astro-ph.CO]]; P. Brax, C. van de Bruck, S. Clesse, A. -C. Davis and G. Sculthorpe, *Phys. Rev. D* **89**, 123507 (2014) [arXiv:1312.3361 [astro-ph.CO]].
- [35] V. Pettorino, L. Amendola and C. Wetterich, *Phys. Rev. D* **87**, 083009 (2013) [arXiv:1301.5279 [astro-ph.CO]].
- [36] T. Basse, O. E. Bjaelde, J. Hamann, S. Hannestad and Y. Y. Y. Wong, *JCAP* **1405**, 021 (2014) [arXiv:1304.2321 [astro-ph.CO]]. S. DeDeo, R. R. Caldwell and P. J. Steinhardt, *Phys. Rev. D* **67**, 103509 (2003) [Erratum-ibid. *D* **69**, 129902 (2004)] [astro-ph/0301284]; M. Takada, *Phys. Rev. D* **74**, 043505 (2006) [astro-ph/0606533]; G. Ballessteros, L. Hollenstein, R. K. Jain and M. Kunz, *JCAP* **1205**, 038 (2012) [arXiv:1112.4837 [astro-ph.CO]].
- [37] C. P. Ma and E. Bertschinger, *Astrophys. J.* **455** (1995) 7, [arXiv:astro-ph/9506072].
- [38] A. Lewis, A. Challinor and A. Lasenby, *Astrophys. J.* **538** (2000) 473 [arXiv:astro-ph/9911177].
- [39] A. Lewis and S. Bridle, *Phys. Rev. D* **66**, 103511 (2002) [arXiv:astro-ph/0205436].
- [40] P. A. R. Ade *et al.* [Planck Collaboration], arXiv:1303.5075 [astro-ph.CO].
- [41] C. L. Bennett *et al.* [WMAP Collaboration], *Astrophys. J. Suppl.* **208**, 20 (2013) [arXiv:1212.5225 [astro-ph.CO]].
- [42] M. Zaldarriaga, S. R. Furlanetto and L. Hernquist, *Astrophys. J.* **608**, 622 (2004) [astro-ph/0311514].
- [43] L. B. Newburgh, G. E. Addison, M. Amiri, K. Bandura, J. R. Bond, L. Connor, J. -F. Cliche and G. Davis *et al.*, arXiv:1406.2267 [astro-ph.IM].
- [44] A. Liu, M. Tegmark, J. Bowman, J. Hewitt and M. Zaldarriaga, arXiv:0903.4890 [astro-ph.CO]; A. Liu, J. R. Pritchard, M. Tegmark and A. Loeb, *Phys. Rev. D* **87**, no. 4, 043002 (2013) [arXiv:1211.3743 [astro-ph.CO]]; J. S. Dillon, A. Liu, C. L. Williams, J. N. Hewitt, M. Tegmark, E. H. Morgan, A. M. Levine and M. F. Morales *et al.*, *Phys. Rev. D* **89**, 023002 (2014) [arXiv:1304.4229 [astro-ph.CO]].